



# Thermochemical energy storage properties of $A_{1-x}Sr_xTO_{3-\delta}$ ( $A = La, Ba, T = Co, Fe, Ni$ ) perovskite oxides

Jialin Qiang<sup>1</sup> · Denghui Wang<sup>1</sup> · Heng Chu<sup>1</sup> · Yuping Huang<sup>1</sup>

Received: 2 March 2023 / Accepted: 5 July 2023 / Published online: 13 July 2023  
© Akadémiai Kiadó, Budapest, Hungary 2023

## Abstract

A series of  $La_{1-x}Sr_xTO_{3-\delta}$  ( $T = Fe, Co, Ni$ ) with different elements at B-site and  $Ba_{1-x}Sr_xCoO_{3-\delta}$  doped with Sr at A-site were prepared by sol–gel method. The samples were tested by synchronous thermal analyzer in air, and the effects of calcination temperature, B-site element type, Sr doping amount on the synthesis and thermal chemical energy storage performance of perovskite oxides were investigated. Through the experiment, we obtained the following main conclusions. (1) In the series of perovskite oxides studied in this article, the higher the calcination temperature required to prepare the samples, the higher the purity and crystallinity of the samples. The samples prepared at higher calcination temperature showed better cycle stability and reversibility in the redox reaction process. (2)  $La_{1-x}Sr_xNiO_{3-\delta}$  samples were not applicable to thermochemical energy storage system. In  $La_{1-x}Sr_xFeO_{3-\delta}$  samples,  $La_{0.1}Sr_{0.9}FeO_{3-\delta}$  exhibited the best energy storage effect. However, compared with  $La_{1-x}Sr_xCoO_{3-\delta}$  samples, Co-based perovskite oxide exhibited more advantages as energy storage materials for thermochemical energy storage systems. (3)  $BaCoO_3$  with single phase needed to be doped with Sr at the A-site to improve its structural stability. Sr doping reduced the molecular weight of  $BaCoO_3$  and increased the energy storage density per unit mass of samples. Energy storage performance of  $Ba_{1-x}Sr_xCoO_{3-\delta}$  samples were the better in a series of  $A_{1-x}Sr_xTO_{3-\delta}$  ( $A = La, Ba, T = Co, Fe, Ni$ ). When Sr doping amount was 0.5, the sample possessed the best energy storage performance.

**Keywords** Perovskite oxides · Air · Thermochemical energy storage · Doping

✉ Denghui Wang  
denghuiwang@163.com

<sup>1</sup> State Key Laboratory of Multiphase Flow in Power Engineering, School of Energy and Power Engineering, Xi'an Jiaotong University, No. 28 Xianning West Rd, Xi'an 710049, China

## Introduction

The fluctuating price of traditional fossil energy and the outstanding contradictions between the environmental pollution problems caused by fossil fuel burning and the goals of "carbon peaking, carbon neutralization" make the exploitation and use of traditional energy questioned, and the consequent rise of low-carbon green energy is widely concerned by people [1, 2]. Actively adjusting the energy structure and promoting the development of renewable energy is an inevitable choice for the sustainable development of human society [3]. Solar energy has the advantages of rich reserves, wide distribution and renewable energy, which is undoubtedly one of the clean energy sources to reduce fossil energy consumption. Due to the influence of season, climate, weather and other factors, solar energy is intermittent and unstable [4]. Heat storage technology is the key to achieving efficient and large-scale storage of solar energy, ensuring sustainable supply of solar energy, and solving the instability problem of solar thermal power generation technology [5–7].

Compared with sensible heat energy storage and latent heat energy storage, thermochemistry energy storage is considered to be one of the most potential high-temperature heat energy storage methods because of its greater energy storage density [8]. When metal oxides are used as energy storage materials for the system, high valence metal oxides are reduced to corresponding low valence metal oxides and oxygen at high temperature and absorb heat. When the temperature drops, the low valence metal oxides are oxidized and release heat to realize the storage and release of solar energy [9, 10]. The reaction temperature of the reaction system is relatively high. Therefore, the metal oxides system can store solar energy at a higher temperature, and it is particularly suitable for high temperature thermal energy storage [11]. In addition, thermodynamics, working temperature, energy storage capacity, material cost, reaction kinetics, toxicity and cycling behavior are important factors for the selection of redox pairs of thermochemical energy storage system. At present, the monomeric metal oxides with application prospects mainly include  $\text{Co}_3\text{O}_4/\text{CoO}$ ,  $\text{CuO}/\text{Cu}_2\text{O}$ ,  $\text{Fe}_2\text{O}_3/\text{Fe}_3\text{O}_4$ ,  $\text{BaO}_2/\text{BaO}$  and  $\text{Mn}_2\text{O}_3/\text{Mn}_3\text{O}_4$ , etc. Scholars explored the redox reaction of these monomeric metal oxides through experiments, the results shown that the monomeric metal oxides, as thermochemical energy storage media, had certain defects in storage performance:  $\text{Mn}_2\text{O}_3/\text{Mn}_3\text{O}_4$  and  $\text{CuO}/\text{Cu}_2\text{O}$  were easy to appear sintering phenomenon in the reaction, which led to the end of the reaction. The conversion rate of  $\text{CuO}$  was low. The researches also shown that the heating and cooling rates and reaction condition have influence on  $\text{Co}_3\text{O}_4/\text{CoO}$  and  $\text{BaO}_2/\text{BaO}$  reaction systems [12]. In order to further improve the heat storage and energy storage performance of the monomeric metal oxides, scholars doped other metal elements into the original metal oxides to change their crystal structure, which can overcome the existing problems to a certain extent. Perovskite oxides are more attractive than  $\text{Co}_3\text{O}_4/\text{CoO}$  and doped manganese oxides in thermodynamics as redox materials for Thermochemistry thermal energy storage systems. The general formula for perovskite oxides is  $\text{ABO}_3$  [13]. The A and B sites of this material can

be improved by doping other elements to improve its physical and chemical properties [14, 15]. Therefore, perovskite oxides are widely used as solid electrolytes [16], sensors [17], high-temperature heating materials [18], solid resistors [17], solid fuel cells [18, 19], catalysts [20–23] and thermochemistry energy storage materials [24, 25] due to their structural characteristics. When perovskite oxide is used as the medium of metal oxide thermochemistry heat energy storage system, the corresponding reversible chemical reaction is used to realize the storage and release of heat. They are suitable for higher temperature thermochemistry energy storage systems and require smaller storage tanks. Its structure contains a large number of oxygen vacancies, and can absorb and release oxygen through reversible redox at high temperature. In addition, before and after the Redox, the crystal structure of the material basically remains unchanged, and there is no phase change between different crystal structures, which leads to small volume changes during the absorption and release of oxygen. Therefore, perovskite oxide can show good redox cycle repeatability, and has certain potential as an energy storage material for solar redox thermochemistry thermal storage system [26]. Laurie et al. [9] found some results by thermogravimetric experimental study of  $\text{CaMnO}_{3-\delta}$ ,  $\text{SrMnO}_{3-\delta}$ ,  $\text{Ca}_{0.5}\text{Sr}_{0.5}\text{MnO}_{3-\delta}$  and  $\text{Ca}_{0.5}\text{Sr}_{0.5}\text{Mn}_{0.5}\text{Fe}_{0.5}\text{O}_{3-\delta}$ .  $\text{CaMnO}_{3-\delta}$  released oxygen when it was heated in Ar atmosphere at 1000 °C, which resulted in a loss-weight of 4.75%. However, when the temperature cooled to 600 °C under 20%  $\text{O}_2$ , the oxidation process hardly absorbed oxygen, and the quality of sample did not increase. For  $\text{SrMnO}_{3-\delta}$ , the reduction of it in air can take place when the temperature was raised.  $\text{Ca}_x\text{Sr}_{1-x}\text{MnO}_{3-\delta}$  was produced by replacing part of Sr with Ca, when  $x$  increased from 0.25 to 0.75, the reaction enthalpy of the material increased from 102 kJ/kg to 266 kJ/kg.  $\text{Ca}_{0.5}\text{Sr}_{0.5}\text{MnO}_{3-\delta}$  can be used for thermochemical energy storage, and the oxygen uptake and release of the material were reduced when the reaction atmosphere changed from Ar to 20%  $\text{O}_2$ .  $\text{Ca}_{0.5}\text{Sr}_{0.5}\text{Mn}_{0.5}\text{Fe}_{0.5}\text{O}_{3-\delta}$  was obtained by doping Fe in B-site, but its redox ability was not further improved. When the series of samples were used in the thermochemical heat storage system, the reduction process needed to be carried out in an inert atmosphere. Imponenti et al. [27] used TGA analysis to study materials partially substituted at the A and B sites of Ca-Mn based perovskite oxides under nitrogen and air exchange atmospheres. Compared with the undoped  $\text{CaMnO}_{3-\delta}$  samples, the materials doped at A and B sites exhibit good redox cycling ability. Among them, the perovskite obtained by doping 5% Sr at the A site has the best redox performance. The reason for this phenomenon may be that the cubic perovskite structure of undoped  $\text{CaMnO}_{3-\delta}$  is partially decomposed into  $\text{CaMn}_2\text{O}_{4-\delta}$  and  $\text{Ca}_2\text{MnO}_{4-\delta}$  phases at a high temperature of 1000 °C [28]. A small amount of Sr doping can inhibit its decomposition, allowing the doped material to be reduced and oxidized more quickly. Bulfin et al. [29] conducted TGA analysis on  $\text{Ca}_{0.8}\text{Sr}_{0.2}\text{MnO}_3$  and  $\text{CaMnO}_3$ . They found that  $\text{Ca}_{0.8}\text{Sr}_{0.2}\text{MnO}_3$  was easier to be reduced than  $\text{CaMnO}_3$ , and  $\text{Ca}_{0.8}\text{Sr}_{0.2}\text{MnO}_3$  showed faster reaction kinetics in the reaction process. Sr doping may improve the cubic structure of perovskite, and enhance the performance of  $\text{Ca}_{0.8}\text{Sr}_{0.2}\text{MnO}_3$ . The thermal chemical energy storage of perovskite oxides has been studied mainly in vacuum, reduction or inert atmosphere. To achieve corresponding reaction atmosphere, equipment and

vacuum pump shall be added to blow inert gas into the system, which inevitably complicates the system and increases operating costs. In order to solve the problem, to find perovskite oxides with good heat storage and energy storage effects under air conditions is a main research direction in the field. Gokon et al. [30] tested the thermodynamic performance of  $\text{La}_{0.5}\text{Sr}_{0.5}\text{MnO}_{3-\delta}$ ,  $\text{La}_{0.5}\text{Sr}_{0.5}\text{FeO}_{3-\delta}$ ,  $\text{La}_{0.5}\text{Sr}_{0.5}\text{CoO}_{3-\delta}$  and  $\text{La}_{0.5}\text{Sr}_{0.5}\text{B}_1\text{B}_2\text{O}_{3-\delta}$  ( $\text{B}_1, \text{B}_2 = \text{Al, Fe, Cr}$ ). The results showed that the net weight change of  $\text{La}_{0.5}\text{Sr}_{0.5}\text{CoO}_{3-\delta}$  was the largest and its activity of redox reaction was the best. The net weight changes of  $\text{La}_{0.5}\text{Sr}_{0.5}\text{B}_1\text{B}_2\text{O}_{3-\delta}$  ( $\text{B}_1, \text{B}_2 = \text{Al, Fe, Cr}$ ) in the redox process were very small, indicating that the series of materials had poor reactivity and slow reaction kinetics. Salles et al. [31] proceeded thermogravimetric analysis on the powder of  $\text{CaTi}_{0.9}\text{Fe}_{0.1}\text{O}_{3-\delta}$  in air and hydrogen, it was found that the weight loss of the sample in hydrogen was significantly greater than that in air.

Bak et al. proposed that the functional properties of  $\text{La}_x\text{Sr}_{1-x}\text{CoO}_{3-\delta}$  series perovskite oxide materials are determined by their defect chemical properties. Scholars have studied and derived defect chemistry models suitable for specific properties of  $\text{La}_x\text{Sr}_{1-x}\text{CoO}_{3-\delta}$  series samples, and conducted in-depth research on the defect model of the materials [32]. In this paper, the thermogravimetric analysis of perovskite oxide and some characterization methods were used to explore the influence of different element composition and doping at A and B sites on the solar thermochemistry energy storage performance of the material. In previous studies, the thermochemistry energy storage performance of a series of  $\text{La}_x\text{M}_{1-x}\text{CoO}_{3-\delta}$  ( $\text{M} = \text{Ba, Sr and K}$ ) perovskite oxides was investigated in air. It was found that Ba and Sr doping can improve the energy storage performance of  $\text{LaCoO}_3$ , while Ba doped samples exhibit better reaction rate and heat storage and release. And the effects of factors such as the type of complexing agent and calcination temperature were explored [33, 34]. On the basis of this research, in order to explore which kind of perovskite oxides of composition of elements have better thermochemical energy storage performance in air,  $\text{A}_{1-x}\text{Sr}_x\text{TO}_{3-\delta}$  ( $\text{A} = \text{La, Ba, T} = \text{Co, Fe, Ni}$ ) were synthesized by sol–gel method in this paper. The results and reasons of the effects of calcination temperature, type of A-site and B-site elements, and doping amount of Sr on the synthesis and energy storage performance of samples were studied by thermogravimetric test and characterization analysis.

## Experimental section

### Preparation method

Firstly, according to certain stoichiometric ratio, lanthanum nitrate hexahydrate, barium nitrate, strontium nitrate, cobalt nitrate hexahydrate, ferric nitrate hexahydrate and nickel nitrate hexahydrate were weighed by electronic scales (0.001 g, JA2003) and dissolved in deionized water. An appropriate amount of citric acid and ethylene glycol were added in the mixed nitrate solution. The solution was heated and stirred on a heat collection constant temperature heating magnetic stirrer (DF-101S) to form gel. The gel is dried in an electric blast drying furnace

(101-0A) to form a dry gel. Then put the dry gel into muffle furnace (STM-8–10, STM-8–12) for calcination. Perovskite oxides of  $A_{1-x}Sr_xTO_{3-\delta}$  ( $A = \text{La, Ba, T} = \text{Co, Fe, Ni}$ ) were obtained by grinding, and the abbreviations of the samples were AS1-xxT ( $A = \text{L, B, T} = \text{C, F, N}$ ). In AS1-xxT-800, 800 indicates that the sample is prepared at 800 °C.

## Thermal analysis

In this experiment, the oxidation and reduction performance of perovskite oxides were evaluated by the synchronous thermal analyzer STA449F3. In each step, the weight change cause by the release and absorption of oxygen is defined as:

$$\omega = \frac{m - m_i}{m_i} \quad (1)$$

Here  $m_i$  is the initial weight of the sample powder, and  $m$  is the weight at time  $t$ .  $\omega$  is calculated from the measured weight of the sample in the instrument.

The principle of synchronous thermal analyzer testing is described as: the sample to be tested is put into an alumina crucible. In the process of furnace temperature rise, the sample occurs endothermic reduction reaction and releases oxygen, which leads to the weight loss of the sample. During the cooling process, the sample occurs exothermic oxidation reaction and absorbs oxygen, therefore, the weight of the sample increases. The TG curve is obtained by plotting the relationship between the weight change of the sample and time. The thermogravimetric curve of the sample is obtained by mapping the weight change  $\omega$  with time. The DTG curve reflecting the reaction rate in the reduction and oxidation process is obtained by the first derivative of the TG curve or the thermogravimetric curve. For the data corresponding to the endothermic and exothermic peaks on the DSC curve, integrate on the X axis (time axis) to get the area of the peaks, and then obtain the heat absorption and release of the sample. By comparing the net weight change, reaction rate and the areas of endothermic and exothermic peaks of the samples, the thermochemical energy storage performance of the samples can be reflected.

In this experiment, the reaction atmosphere is air. The pure oxygen and nitrogen are mixed according to the ratio of 20% and 80%. The gas flow rates are 10 mL/min and 40 mL/min. The reaction temperature program settings for this experiment are consistent with those in reference [33, 34], and will not be elaborated in this article.

## Sample characterization

### X-ray diffractometer

In this paper, the crystal structure of perovskite oxide was analyzed by X-ray diffractometer (XRD, D8 ADVANCE, Germany).

## Field emission scanning electron microscopy

By using field emission scanning electron microscopy (SEM/EDS, JEOL 7800F, Japan) to qualitatively and quantitatively analyze the elements contained in the tested sample, the micro external morphology of the sample can also be observed.

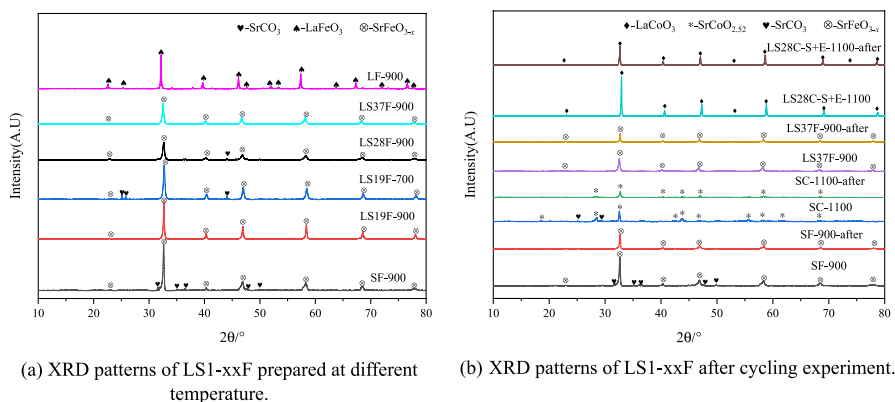
## X-ray photoelectron spectroscopy

X-ray photoelectron spectroscopy (XPS, Thermo Fisher ESCALAB Xi+, USA) can be used to test the elemental composition, proportion, and valence distribution of elements in samples. This article measures and analyzes the full spectrum of the sample and elements such as O1s, Sr3d, Co2p, C1s, and Ba3d. After C1s correction, the data is divided into peaks and calculated. The XPS testing of the sample in this article involves the preparation process of the sample. The powder sample is made into a dense and smooth tableting. The sample tableting is analyzed and tested. This method can improve the signal strength of the test. The flat and uniform area in the middle of the tableting is scanned to obtain reliable analytical data. The scanning depth used in this test is within 10 nm of the sample surface.

## Results and discussion

### Effect of different B-site elements on energy storage performance of $\text{La}_{1-x}\text{Sr}_x\text{TO}_{3-\delta}$ (T = Fe, Co, Ni)

Fig. 1 shows the XRD patterns of LS1-xxF. In Fig. 1a, the characteristic diffraction peaks of the sample without Sr doping is  $\text{LaFeO}_3$  perovskite oxide, which is consistent with the standard card in MDI Jade 6.0 software. The characteristic diffraction peaks of Sr doped samples are similar to the XRD pattern of  $\text{SrFeO}_{3-x}$ . LS19F prepared at 700 °C also has the impurity of  $\text{SrCO}_3$  in the sample because of the

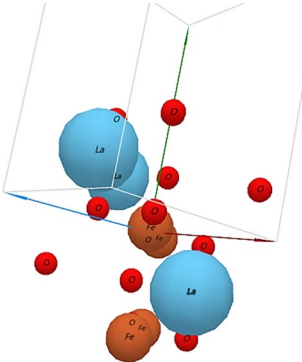
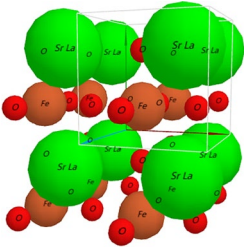
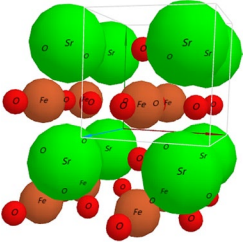


**Fig. 1** XRD patterns of LS1-xxF

low calcination temperature. The presence of impurities may be an important reason for why the loss-weight rate of LS19F-700 in the first reduction process is higher than LS19F-900 in the thermogravimetric analysis experiment. There are very weak  $\text{SrCO}_3$  impurity peaks in the XRD spectra of SF and LS28F prepared at 900 °C, which may be mixed in the sample preparation or testing process. The other samples only contain a single perovskite oxide phase, and the corresponding characteristic peaks are sharp. In a series of samples doped with Sr, compared with the position of characteristic peak of  $\text{SrFeO}_{3-x}$ , since the radius of  $\text{La}^{3+}$  is smaller than that of  $\text{Sr}^{2+}$ , the characteristic peak of the sample shifts to a large angle with the increase of La content. This can be ascribed to the successive replacement of smaller  $\text{La}^{3+}$  cation (1.36 Å) by bigger  $\text{Sr}^{2+}$  cation (1.44 Å), leading to the expansion of perovskite unit cell [35]. In Fig. 1b, by comparing the XRD patterns of SF, LS37F, SC, and LS28C before and after cycling experiment, we find that a small amount of impurities mixed in the original samples disappear completely after cyclic thermogravimetric testing. The characteristic peak intensity of perovskite oxide in the samples weaken, but no new phase appears. This phenomenon indicates that these samples will not decompose during cycling and have a stable structure. Further analysis by XRD reveals the crystal structure and corresponding crystal lattice parameters of LS1-xxF, as shown in Table 1. Through Sr doping, the orthorhombic crystal structure of  $\text{LaFeO}_3$  gradually transforms into a cubic crystal structure of  $\text{La}_{1-x}\text{Sr}_x\text{FeO}_{3-\delta}$  ( $x=0.9, 1.0$ ).

The synchronous thermal analyzer is used to determine the heat treatment temperature of the dry gels. The thermal stability analysis curves of the dry gels of  $\text{La}_{1-x}\text{Sr}_x\text{TO}_{3-\delta}$  ( $T=\text{Fe, Ni}$ ) are shown in Fig. 2. It can be seen from Fig. 2a that the weight loss of dry gel is mainly divided into four stages through analysis. The first stage of dry gel is from room temperature to 124 °C. Due to the evaporation of free water contained in the sample, the loss-weight rate at this stage is about 5%, and a weak endothermic peak appeared at about 108 °C on the DSC curve, representing the evaporation of water. The second stage is from 124 °C to 574 °C. There is 68% of loss-weight rate on the TG curve. The first part is due to the intramolecular dehydration of citric acid and nitrate. From the DSC curve, there is an exothermic peak at 254 °C. The second part is due to the intense combustion of citric acid, which decomposed and released  $\text{CO}_2$  and  $\text{H}_2\text{O}$ . At the same time, the DSC curve show that the process is accompanied by a generous amount of heat release. Temperature from 574 °C to 800 °C is the third stage. The weight loss at the stage is relatively slow. There is a slight endothermic peak on the DSC curve, which may be due to the fact that nitrate started to decompose violently to generate oxides at the temperature and reacted with  $\text{CO}_2$  generated by citric acid combustion to generate carbonates. Then, various compounds interact with each other to lose oxygen and combine to form perovskite type composite oxides. In other words, the stage is the process of initial formation of crystal nucleus of LS1-xxF perovskite oxides. The fourth stage occurred at 800~1200 °C, there is basically no weight loss and heat change, but the baseline of the DSC curve kept moving up, corresponding to the constant increase of the specific heat capacity of the product. It means that the perovskite structure of LS1-xxF has been formed below 900 °C, and the lattice is gradually improved during the stage. Therefore, 900 °C is the appropriate calcination temperature for the series of LS1-xxF perovskite oxides. According to the analysis of Fig. 2b and the

**Table 1** Crystal structure and corresponding crystal lattice parameters of LS1-xxF

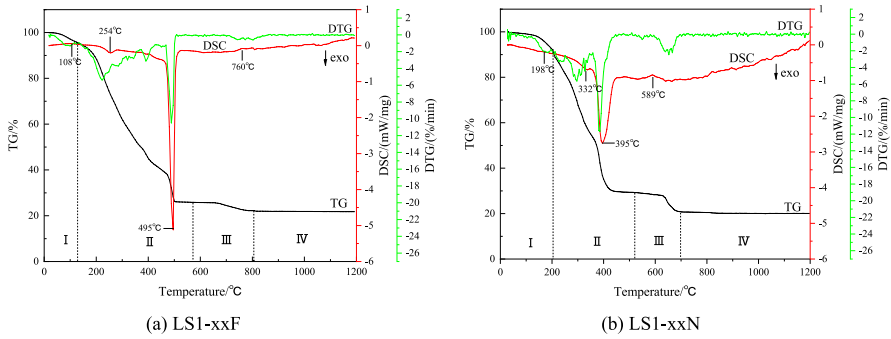
Crystal structure	a (Å)	b (Å)	c (Å)	$\alpha$	$\beta$	$\gamma$
LaFeO <sub>3-<math>\delta</math></sub>  Orthorhombic crystal structure	5.560	7.860	5.560	90.00°	90.00°	90.00°
La <sub>0.1</sub> Sr <sub>0.9</sub> FeO <sub>3-<math>\delta</math></sub>  Cubic crystal structure	3.880	3.880	3.880	90.00°	90.00°	90.00°
SrFeO <sub>3-<math>\delta</math></sub>  Cubic crystal structure	3.860	3.860	3.860	90.00°	90.00°	90.00°

(The red, green, and blue axes in the crystal structure of samples represent the a, b, and c axes)

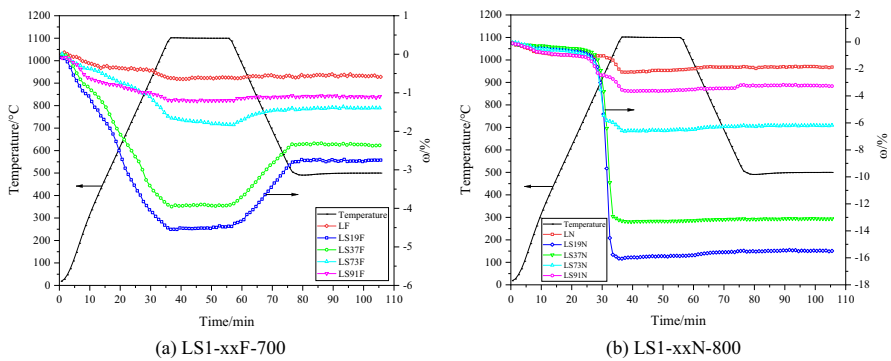
literature [34], the process of weight loss of the dry gel of LS1-xxN and LS1-xxC also can be divided into four stages, and the suitable calcination temperatures of them are 800 °C and 1100 °C.

Fig. 3 shows the one cycle thermogravimetric TG curves of LS1-xxF-700 and LS1-xxN-800. It can be seen from Fig. 3a that LF has almost no reduction and oxidation processes, and there is no obvious weight change. The net weight changes of LS19F, LS37F, LS73F and LS91F are 1.80%, 1.64%, 0.43% and 0.12%. It means that Sr doping can enhance the redox activity of LaFeO<sub>3</sub>, and the net weight changes of the doped samples increase with the increase of Sr doping amount. From TG





**Fig. 2** The thermal stability analysis curves of the dry gels of  $\text{La}_{1-x}\text{Sr}_x\text{NO}_{3-\delta}$  ( $N = \text{Fe}, \text{Ni}$ ). (The reaction atmosphere is air. The temperature of thermogravimetric test is between room temperature and 1200 °C, and the rate of rise and fall of temperature used in the experiment is 10 °C /min.)



**Fig. 3** TG curves of one cycle for LS1-xxF prepared at 700 °C and LS1-xxN prepared at 800 °C. (The reaction atmosphere is air. The temperature of thermogravimetric test is between 500 and 1100 °C, and the rate of rise and fall of temperature used in the experiment is 30 °C /min.)

curves of the one cycle for a series of LS1-xxN samples doped with Sr in Fig. 3b, during the temperature rise and reduction process of LN, the TG curve has a slow weight loss phenomenon from room temperature to 835 °C. When the temperature continued to rise to 1100 °C, a loss-weight rate of LN is about 1.5%. In the cooling stage, there is almost no gain-weight rate in the TG curve. TG curves of Sr doped samples show that the loss-weight rates of the series of perovskite oxides in the reduction process increase gradually with the increase of Sr doping amount. The gain-weight rates of the samples after doping have not been improved, therefore, Sr doping has no effect on the oxidation reaction of LS1-xxN samples.

Fig. S1 shows the TG curves of cycling experiment for LS1-xxF. By comparing Figs. S1d and S1f, it can be seen that the loss-weight rate of LS19F-700 in the first reduction process is greater than LS19F-900. The reason may be that the samples calcined at a lower temperature contain impurities. The impurities are decomposed by heating during thermogravimetric analysis, and a large loss-weight rate is

generated in the first reduction process. For the samples calcined at 900 °C, LF still unable to conduct redox reaction. The loss-weight rates of other samples decrease in the first reduction process. In the subsequent cycling experiment, maintain relatively stable loss-weight rates and gain-weight rates. During each cycle, the net weight changes of the samples fluctuate within a small range because of the errors of mass determination. The net weight changes of LS37F, LS28F, LS19F and SF are  $1.53 \pm 0.01\%$ ,  $1.57 \pm 0.02\%$ ,  $1.72 \pm 0.01\%$  and  $1.10 \pm 0.03\%$ , which means that the samples prepared at 900 °C have good cycle stability and reversibility. Therefore, when Sr doping amount is less than and equal to 0.9, with the increase of Sr doping amount, the net weight changes of the series of samples show a trend of increasing. However, the net weight change of SF is smaller than that of LS19F, in other words, the presence of a small amount of La is instrumental in producing the greater net weight change for LS1-xxF. By comparing the data of thermogravimetric analysis of LS1-xxF and LS1-xxC [33], except that the net weight changes of the TG curves of LS28C and LS19F are similar, the net weight changes of the TG curves of the series of perovskite oxides with Co at B-site are greater than those of the samples with Fe at B-site. Therefore, a series of perovskite oxides containing Co have more advantages in thermochemical heat storage systems.

Fig. S2a is the reaction rate diagram of the cycling experiment for the sample prepared at 900 °C. Except that the reaction rate diagram of SF has small reduction reaction rate peak, there are no obvious redox reaction rate peaks in the reaction rate curves of the other samples before and after Sr doping. These results indicate that Sr doping has little positive effect on the reaction kinetics of the samples. As shown in Fig. S2b, taking the DSC curve of SF as an example, the DSC curves of LS1-xxF have no obvious endothermic and exothermic peaks. From the literature [33], we know that the reaction rate diagram and the DSC curves of LS1-xxC are the similar with those of LS1-xxF. However, the reaction kinetics and heat absorption and release capacity of LB1-xxC are better than LS1-xxC and LS1-xxF.

Fig. S3 shows the results of EDS qualitative and semi-quantitative analysis and SEM test of LS19F prepared at 900 °C. The different colors in Fig. S3a represent the distribution of La, Sr, Fe and O. The atoms are evenly dispersed and Sr element is doped into the lattice of perovskite oxide. The percentages of La, Sr and Fe atoms in the sample determined by EDS are 5.02%, 43.23% and 51.25%. The ratio of (La + Sr)/Fe is 0.94, which is close to the standard value of 1, indicating that the components of the sample are uniformly mixed during the preparation process. The SEM image of LS19F is shown in Fig. S3b. The particles are in a block structure with uniform size, and no agglomeration occurs between particles.

The XPS analysis results of SF, LS19F and LS28F are shown in Fig. 4. Fig. 4a shows the C 1s XPS spectrum of LS1-xxF. Firstly, peak fitting is performed on C 1s. There is a low intensity peak at 288–290 eV, which may indicate carbonization of the powder or non-uniformity of the material. Then, full spectrum carbon correction is performed and the spectra of other elements are analyzed. In Fig. 4b, the samples contain lattice oxygen  $O_{\beta}$ , adsorbed oxygen  $O_{\alpha}$ , and adsorbed water molecule  $O_{\gamma}$  (a kind of adsorbed oxygen). The relative contents of ( $O_{\alpha} + O_{\gamma}$ ) of the three samples are 62.32%, 87.09% and 80.29%. The higher the proportion of adsorbed oxygen, the higher the concentration of oxygen vacancies, which is more conducive

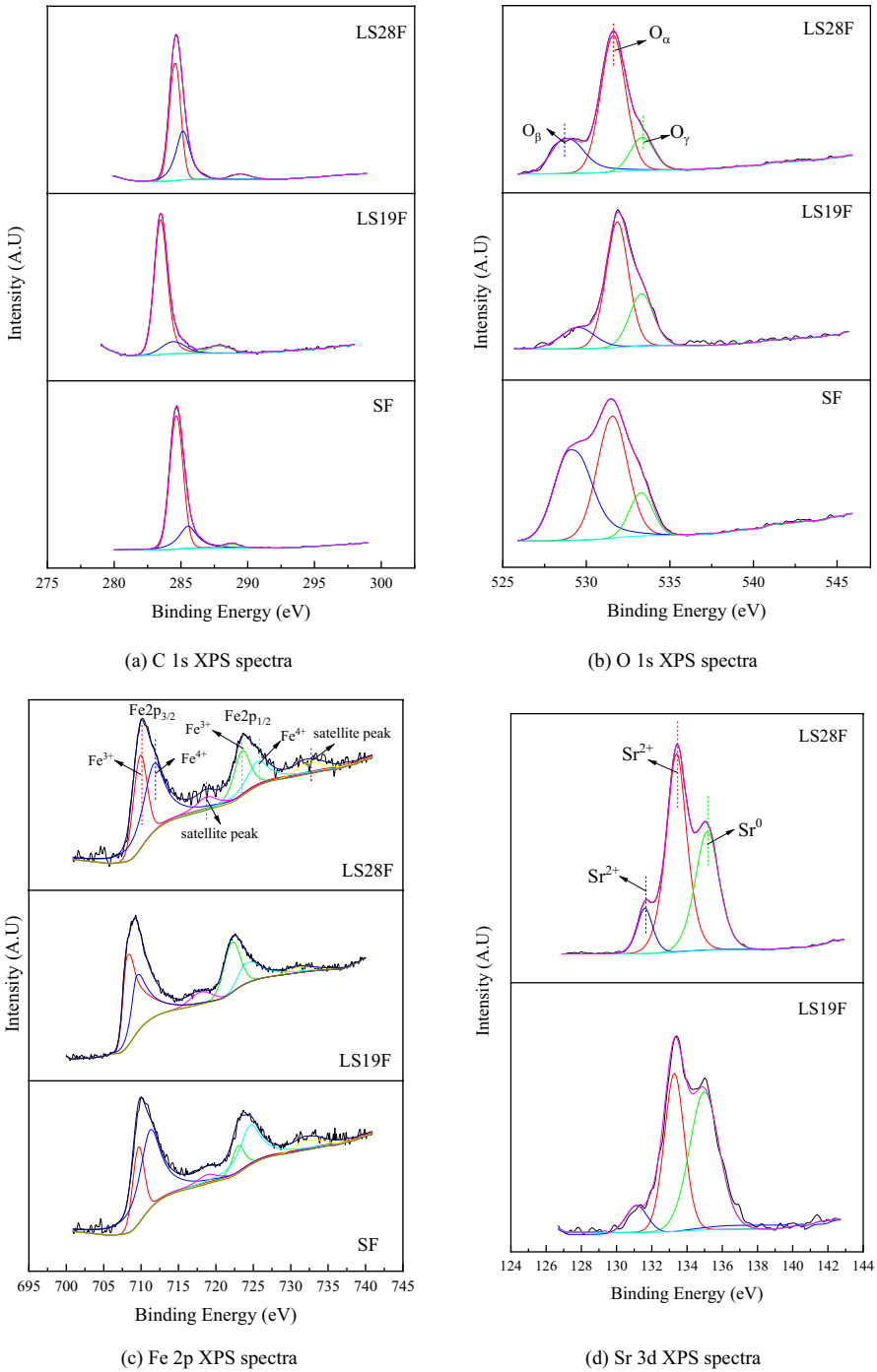


**Fig. 4** XPS spectrum of SF, LS19F and LS28F prepared at 900 °C

to improving the transport performance of oxygen ions [36, 37]. Therefore, LS19F exhibits a higher oxygen vacancy concentration, leading to the large net weight change for LS19F. The conclusion is consistent with the results of thermogravimetric analysis of the sample. Fig. 4c shows the Fe 2p analysis of SF, LS19F and LS28F. The samples have characteristic peaks of Fe<sup>3+</sup> and Fe<sup>4+</sup>. The corresponding binding energies are 709.8 eV, 723.1 eV and 711.9 eV, 725.1 eV [38], and the other two peaks represent satellite peaks. The relative content of Fe<sup>4+</sup> in SF, LS19F and LS28F are 65.37%, 39.84% and 53.95%. In perovskite oxides, the average electricity price at A-site is reduced, when the high valence ion at A-site is replaced by the low valence ion. In order to maintain the electricity neutrality, electricity price compensation must be carried out. There are generally two ways to compensate for valence states: increasing the valence state of B-site ions and increasing the concentration of oxygen vacancies [39]. The increase of oxygen vacancy concentration in the material can further increase the permeability of oxygen, which is conducive to the diffusion and migration of oxygen in the crystal structure of the material. Therefore, the process of releasing and absorbing oxygen in the reduction and oxidation process of the material can be easier, and its redox activity can be improved. The reason why the Fe<sup>4+</sup> content of LS19F is lower than that of LS28F may be that LS19F mainly relies on increasing the concentration of oxygen vacancies to compensate for the valence state. In theory, Fe exists tetravalent in SrFeO<sub>3</sub>, but the sample is very easy to obtain electrons and reach a semi-filled stable structure. Therefore, the coexistence of Fe<sup>3+</sup> and Fe<sup>4+</sup> occur in the sample, and Fe<sup>4+</sup> is dominant [40]. From the Sr 3d XPS spectra in Fig. 4d, we find that the "surface" components of Sr<sup>2+</sup> in LS19F and LS28F are 84.76% and 68.88%, which indicates that the reactivity of LS19F may be better than other samples in this series [41]. The XPS analysis results indicate that the presence of a small amount of La is beneficial for the redox performance of LS1-xxF samples.

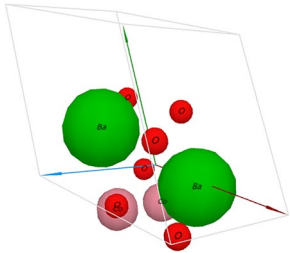
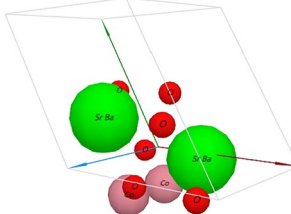
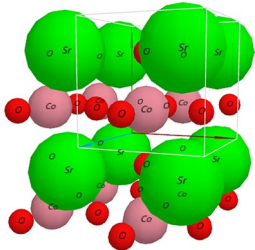
The thermogravimetric analysis results of samples with different elements at B-site and samples doping different elements at A-site [34] show that the element combination of Sr and Ba at A-site and Co at B-site may have better thermochemical energy storage performance.

### Energy storage performance of Ba<sub>1-x</sub>Sr<sub>x</sub>CoO<sub>3-δ</sub>

The XRD patterns of Ba<sub>1-x</sub>Sr<sub>x</sub>CoO<sub>3-δ</sub> prepared at different calcination temperatures are shown in Fig. S7. Fig. S4a shows that there is a characteristic diffraction peak of BaCoO<sub>3</sub> in the patterns of the samples prepared at 800 °C, however, due to the low calcination temperature, many impurities existed in the sample, such as BaCO<sub>3</sub>, Co<sub>3</sub>O<sub>4</sub>. The presence of impurities may be an important reason for the large loss-weight rate in the first reduction process of the sample prepared at the temperature in the thermogravimetric analysis experiment. As shown in Fig. S4b, when the calcination temperature of the samples is increased to 1100 °C, there may still be very weak SrCO<sub>3</sub> impurity peaks in the XRD spectra of some BS1-xxC samples prepared at 1100 °C by operational errors during sample preparation or testing. The pattern of undoped BaCoO<sub>3</sub> is consistent with the standard card

in Jade 6 software. Since the radius of  $\text{Sr}^{2+}$  is smaller than that of  $\text{Ba}^{2+}$ , Sr doping makes the cell parameters of the samples smaller and the crystal plane spacing smaller. Therefore, with the increase of Sr doping amount, the characteristic peaks of the samples shift to a large angle, which means that Sr enters the lattice of perovskite. When  $x$  is greater than or equal to 0.9, the interaction between Sr and Co formed a new phase named  $\text{SrCoO}_{2.5}$  perovskite oxide. In Fig. S4b, by comparing the XRD patterns of BC, BS55C and SC before and after cycling experiment, these three samples are still perovskite oxides before and after the cycling experiment, which means that the structures of the series of samples are stable. Table 2 shows the crystal structure and corresponding crystal lattice parameters of BS1-xxC. When the A-site is entirely occupied by Ba, a hexagonal crystal structure is more likely to appear. The doping of Sr can transform this series of perovskite oxides into a more stable cubic crystal structure [42].

**Table 2** Crystal structure and corresponding crystal lattice parameters of BS1-xxC

	Crystal structure	a (Å)	b (Å)	c (Å)	$\alpha$	$\beta$	$\gamma$
$\text{BaCoO}_{3-\delta}$	 Hexagonal crystal structure	5.610	5.610	4.770	90.00°	90.00°	120.00°
$\text{Ba}_{0.5}\text{Sr}_{0.5}\text{CoO}_{3-\delta}$	 Hexagonal crystal structure	5.540	5.540	4.240	90.00°	90.00°	120.00°
$\text{SrCoO}_{3-\delta}$	 Cubic crystal structure	3.830	3.830	3.830	90.00°	90.00°	90.00°

(The red, green, and blue axes in the crystal structure of samples represent the a, b, and c axes)

Sr element is doped at A-site of  $\text{BaCoO}_3$  to form BS1-xxC. We explored the influence of calcination temperature and Sr doping amount on the thermochemical energy storage performance of BS1-xxC. Fig. S5 shows the thermal stability analysis curve of dry gel of BS1-xxC, and the analysis process of BS1-xxC is similar to that of LS1-xxF, the proper calcination temperature of BS1-xxC is 1100 °C.

Through the cycling experiment on the samples prepared at 800 °C in Figs. S6a–d, we find that the loss-weight rates in the first reduction process of all samples are much larger than the gain-weight rates in the oxidation process, and the net weight changes of BC increases after several cycles. The reason for the phenomenon may be the interference of external factors on the instrument or the instability of the structure of these samples, which leads the decomposition of the samples during the cycling experiment. The net weight changes of BS73C, BS46C and BS37C do not increase with the increase of the number of cycles, but decrease from 2.08% to 1.95%, from 1.94% to 1.68% and from 1.83% to 1.72%. The reason may be that the existence of Sr can stabilize the structure of BS1-xxC. The phenomenon that there are large loss-weight rates of samples in the first reduction process and the net weight changes of them decrease with the increase of the number of cycles may be caused by the decomposition of impurities. Fig. S6 also shows that the loss-weight rates of the samples prepared at 1100 °C in the first reduction process of the cycling experiment are much smaller than those of the samples prepared at 800 °C, and the loss-weight rates and gain-weight rates of the samples in the subsequent cycle process remained relatively stable, which means that the perovskite oxides of BS1-xxC have good redox stability and reversibility. The existence of quality measurement errors results in small fluctuations in the net weight changes during sample cycling. The net weight changes of BC, BS73C, BS55C, BS37C, BS19C and SC are  $1.93 \pm 0.03\%$ ,  $1.98 \pm 0.01\%$ ,  $2.00 \pm 0.01\%$ ,  $1.89 \pm 0.03\%$ ,  $1.81 \pm 0.02\%$  and  $1.39 \pm 0.01\%$ . When the Sr doping amount  $x$  are 0.5 and 0.3, the net weight changes of the samples are larger than that of the undoped sample. On the basis of the same net weight change, since the relative molecular weight of Sr (87.62) is less than Ba (137.3), the doping of Sr can reduce the molecular weight of perovskite oxide and increase the energy storage density per unit mass. For the perovskite oxides of BS1-xxC,  $\text{Sr}^{2+}$  and  $\text{Ba}^{2+}$  are divalent cations. In theory, Sr doping does not increase the oxygen vacancy concentration in perovskite oxides.

Table 3 shows the calculation results of tolerance factor  $t$  of BS1-xxC samples prepared at 1100 °C before and after doping. Generally, when the value of  $t$  is greater than 0.75 but less than 1.00, the perovskite structure can exist stably. Some studies show that the stability range of cubic perovskite structure is  $0.95 < t < 1.04$ . When the A-site is occupied by  $\text{Ba}^{2+}$ , and the value of  $t$  is greater than 1.04, therefore, it is more likely to have a structure similar to hexagonal phase. With the increase of Sr doping amount,  $t$  gradually approaches 1, which shows that the difference in ion radius between  $\text{Sr}^{2+}$  (1.44 Å) and  $\text{Ba}^{2+}$  (1.61 Å)

**Table 3** Tolerance factor  $t$  for the BS 1-xxC samples prepared at 1100 °C

Samples	BC	BS73C	BS55C	BS37C	BS19C	SC
$t$	1.048	1.031	1.019	1.007	0.995	0.989

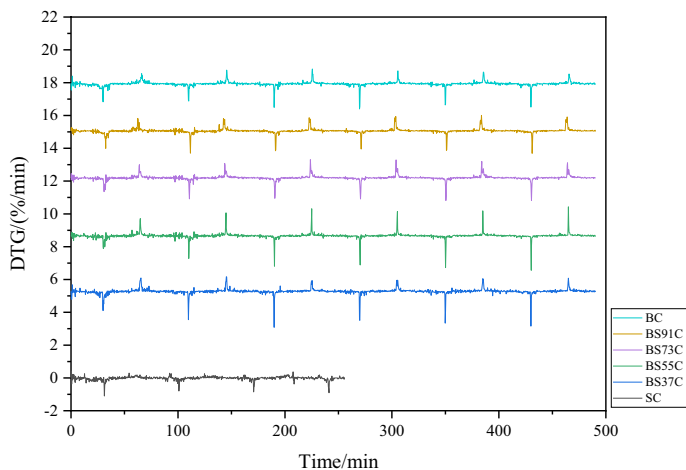


**Fig. 5** DTG diagram of thermogravimetric cycling experiment for BS1-xxC prepared at 1100 °C. (The reaction conditions are the same as Fig. S1.)

can reduce the lattice distortion of  $\text{BaCoO}_3$ , and improve the structural stability of  $\text{BaCoO}_3$ , which induces the absorption or release of oxygen [30].

From the DTG curves of the series of samples prepared at 1100 °C in Fig. 5, it can be seen that the redox reaction rates of the samples containing Ba have obvious peaks, indicating that the reaction kinetics of these samples is good. With the increase of Sr doping amount, the reaction rates of the series of samples first accelerate and then slow down. Among them, the reduction reaction rate of BS37C is the fastest and slightly faster than that of BS55C. The sample containing only Sr has almost no peak of reduction reaction rate. The oxidation reaction rate of BS55C is obviously faster than that of other samples.

Take the DSC measurement results of BS37C, BS19C and SC prepared at 1100 °C for example, as shown in Fig. S7. By integrating the areas of heat absorption and release peaks, it can be seen that the average heat absorption amount of BC, BS73C, BS55C, BS37C, BS19C and SC in the series of perovskite oxides are 10.2 J/g, 8.4 J/g, 21.6 J/g, 16.2 J/g, 12.6 J/g and 10.4 J/g. BS55C has the largest heat absorption amount. The average heat release amount of these samples are 14.4 J/g, 3.6 J/g, 9.6 J/g, 13.8 J/g and 15.6 J/g, but there is no corresponding exothermic peak in the DSC curve of SC. BS19C has the largest heat release amount.

In general, BS1-xxC series samples exhibit positive redox reactivity, reaction cycle stability and repeatability, reaction kinetic characteristics, and heat storage and release capacity, which are suitable for using as energy storage materials for thermochemical energy storage systems.

Table 4 lists the percentage of metal atoms in BS1-xxC determined by EDS. By analyzing the atomic ratios at three different positions in the samples, the average atomic ratios of the samples are obtained. Due to human factors such as operational errors during sample preparation, the atomic ratio in the sample is not completely consistent with the standard atomic ratio, but the content of

**Table 4** Compositional analysis of BS1-xxC by SEM/EDS analysis

Samples		Atomic ratio (%)				Average atomic ratio (%)
		Ba	Sr	Co	(Ba + Sr)/Co	(Ba + Sr)/Co
BC-1100	Nominal	50.00	0.00	50.00	1.00	1.00
	EDS	52.90	52.21	0.00	47.10	1.12
		52.03		0.00	47.79	1.09
			0.00	47.97	1.08	
BS73C-1100	Nominal	35.00	15.00	50.00	1.00	1.00
	EDS	38.03	15.84	46.12	1.17	1.17
		38.40	15.74	45.86	1.18	
		37.96	15.67	46.37	1.16	
BS55C-1100	Nominal	25.00	25.00	50.00	1.00	1.00
	EDS	23.12	25.56	51.31	0.95	0.94
		22.43	24.79	52.78	0.89	
		24.63	25.21	50.19	0.99	
BS37C-1100	Nominal	15.00	35.00	50.00	1.00	1.00
	EDS	12.40	35.82	51.78	0.93	0.94
		16.34	31.97	51.69	0.93	
		14.88	34.20	50.92	0.96	

each element is similar to the proportion of elements added during the preparation process.

Fig. S8 shows the microscopic morphology characteristics of BS1-xxC series perovskite oxides prepared at 1100 °C by SEM. It can be seen from Fig. S8a that the particle size of the undoped BC sample is very uneven, and it presents two forms as blocky and needle. The existence of needle particles can provide a larger specific surface area, which may be one of the reasons for their better redox reactivity and reaction kinetics compared with LS1-xxC samples. After Sr doping, the needle-like structure disappears. The particles of BS73C have smooth surface and uniform size. The particles of BS55C and BS37C exhibit an irregular coral structure, and there is adhesion between the particles. The pores of BS55C particles are rich, and the effective specific surface area is large, which is conducive to full contact between gas and particles. Therefore, the sample presents good redox reactivity in a series of doped samples.

From the XPS analysis results of BC, BS55C and BS73C in Fig. S9. Peak fitting and full spectrum carbon correction are performed on C 1s. Then the spectra of other elements are analyzed. The O 1s spectra of the three perovskite samples show two obvious characteristic peaks, which are lattice oxygen  $O_{\beta}$  and surface adsorbed oxygen  $O_{\alpha}$ . The relative contents of  $O_{\alpha}$  reflecting oxygen vacancy concentration are 89.43%, 90.79% and 89.80%, which is consistent with the results of thermogravimetric analysis. The Co 2p spectrum shows that the Co ions of the three are trivalent. The reason is that the doping will not cause the change of the valence state of the B site element, since Sr and Ba are both bivalent ions. In the XPS spectra of Sr, the "surface" components of  $Sr^{2+}$  in BS55C and BS73C are 78.11% and 71.06%, which may be one of the reasons for BS55C with good reactivity.



## Conclusion

1. In the series of perovskite oxides prepared in this article, there were impurities in the samples prepared at a lower calcination temperature, which led to a large loss-weight rates in the first reduction process in the thermal analysis TG curves of the samples. The purity and crystallinity of the samples calcined at higher temperature were higher. The samples shown better cycle stability and reversibility in the redox reaction process.
2. The comparison of three groups of perovskite oxides with elements of Fe, Co and Ni at B-site shown that the reduction process of LS1-xxN samples had a corresponding loss-weight rates, but the oxidation capacity was very poor. The cycling TG curves of LS1-xxF and LS1-xxC obtained by Sr doping maintained stable loss-weight rate and gain-weight rate. With the increase of Sr doping amount, the net weight changes of samples increased first and then decreased. Among them, the relative contents of adsorbed oxygen of LS19F and LS28C were the larger, which led to better energy storage performance for LS19F and LS28C. The net weight changes of other perovskite oxides with Co at B-site were greater than those of samples with Fe at B-site. Therefore, a series of perovskite oxides containing Co possessed more advantages in thermochemical heat storage systems.
3. The structural stability of single-phase  $\text{BaCoO}_3$  was improved by doping at the A and B sites. Although Sr doping did not increase the oxygen vacancy concentration in perovskite oxides, it reduced the lattice distortion of  $\text{BaCoO}_3$ . The structural stability of  $\text{BaCoO}_3$  was improve by Sr doping, which induced the absorption or release of oxygen. In addition, since the relative molecular weight of Sr was less than Ba, the doping of Sr reduced the molecular weight of perovskite oxide and increased the energy storage density per unit mass. Energy storage performance of BS1-xxC samples were the better in a series of  $\text{A}_{1-x}\text{Sr}_x\text{TO}_{3-\delta}$  ( $\text{A} = \text{La}, \text{Ba}, \text{T} = \text{Co}, \text{Fe}, \text{Ni}$ ). When Sr doping amount was 0.5, the sample exhibited the best energy storage performance.

In this paper, the research on the thermochemistry energy storage performance of perovskite oxides in air is still in the stage of laboratory research. The next step of research should be to build a test bench. Through the design of thermochemistry energy storage reactor and other devices, the pilot test research of this material is carried out. It is also necessary to conduct technical and economic feasibility study, safety assessment, cost/benefit analysis on the perovskite oxides thermal energy storage system. The potential of perovskite oxides for thermochemistry energy storage is reflected by integrating the results of various analyses.

**Supplementary Information** The online version contains supplementary material available at <https://doi.org/10.1007/s11144-023-02445-5>.

**Acknowledgements** The present work is supported by the National Natural Science Foundation of China (51906193).

**Data availability** All data, models, and code generated or used during the study appear in the submitted article.

## Declarations

**Conflict of interest** The authors declare that they have no known competing financial interests or personal relationships that could have appeared to influence the work reported in this paper.

## References

1. Wang Z, Ren Y (2010) Utilization status and industrial development of solar energy resources in China. *Resour Ind* 2:89–92. <https://doi.org/10.3969/j.issn.1673-2464.2010.02.018>
2. Wang YP, Xu YS, Liang WY (2002) Review of solar thermal power generation from the perspective of sustainable development strategy. *Sci. Technol. Manag. Res.* 3:92–95. <https://doi.org/10.3969/j.issn.1000-7695.2002.03.032>
3. Panwar NL, Kaushik SC, Kothari S (2011) Role of renewable energy sources in environmental protection: a review. *Renew. Sustain. Energy Rev.* 3:1513–1524. <https://doi.org/10.1016/j.rser.2010.11.037>
4. Chen Y (2010) Application and prospect of concentrating solar energy power plant (CSP) technology. *Power Syst Clean Energy* 26(7):29–33
5. Pinel P, Cruickshank CA, Beausoleil- Morrison I, Wills A (2011) A review of available methods for seasonal storage of solar thermal energy in residential applications. *Renew Sustain Energy Rev* 7:3341–3359. <https://doi.org/10.1016/j.rser.2011.04.013>
6. Du ES, Zhang N, Kang CQ, Miao M (2016) Reviews and prospects of the operation and planning optimization for grid integrated concentrating solar power. *Proc CSEE* 21:5765–5775. <https://doi.org/10.13334/j.0258-8013.pcsee.161251>
7. Pelay U, Luo L, Fan Y, Stitou D, Rood M (2017) Thermal energy storage systems for concentrated solar power plants. *Renew Sustain Energy Rev* 79:82–100. <https://doi.org/10.1016/j.rser.2017.03.139>
8. Prieto C, Cooper P, Fernández AI, Cabeza LF (2016) Review of technology: thermochemical energy storage for concentrated solar power plants. *Renew Sustain Energy Rev* 60:909–929. <https://doi.org/10.1016/j.rser.2015.12.364>
9. André L, Abanades S (2018) Investigation of metal oxides, mixed oxides, perovskites and alkaline earth carbonates/ hydroxides as suitable candidate materials for high-temperature thermochemical energy storage using reversible solid-gas reactions. *Mater Today Energy* 10:48–61. <https://doi.org/10.1016/j.mtener.2018.08.007>
10. Felinks J, Brendelberger S, Roeb M, Sattler C, Pitz-Paal R (2014) Heat recovery concept for thermochemical processes using a solid heat transfer medium. *Appl Therm Eng* 73:1006–1013. <https://doi.org/10.1016/j.applthermaleng.2014.08.036>
11. Wu J, Long XF (2014) Research progress of solar thermochemical energy storage. *Chem Prog* 12:3238–3245. <https://doi.org/10.3969/j.issn.1000-6613.2014.12.018>
12. Zhao MJ, Wang DH, Hui SE, Niu YQ (2020) Research progress of energy storage medium using redox reaction for energy storage. *Thermal Power Gener* 8:19–28. <https://doi.org/10.19666/j.rlfd.202003078>
13. Li YC, Wang XH, Shao JA, Li P, Yang HP, Chen HP (2016) Utilization of pyrolytic char derived from bamboo chips for furfural removal: kinetics, isotherm, and thermodynamics. *Energy Sources Part A* 38:1520–1529. <https://doi.org/10.1080/15567036.2014.940093>
14. Yu JF, Luo LH, Cheng L, Wang LY, Xia CK, Xu X, Yu YZ (2020) Research progress of solid oxides fuel cell materials. *Acta Ceram Sin* 5:613–626. <https://doi.org/10.13957/j.cnki.tcxh.2020.05.003>
15. Deng JG, Wang GZ, Zhang YJ, Dai HX, He H, Qiu WG, Zi XH (2006) Preparation and photocatalytic performance of perovskite oxides. *Chin J Rare Earth* 6:81–93. <https://doi.org/10.3321/j.issn:1000-4343.2006.z2.020>
16. Li DG, Zhang HY, Zhang HF, Guo QQ, Cao MC (2006) Progress in research and application of perovskite composite oxides. *Mater Rev* 6:296–299. <https://doi.org/10.3321/j.issn:1005-023X.2006.z1.095>
17. Wang GJ, Qin YN, Ma Z, Wang YC (2005) Perovskite composite oxides materials. *Chin Chem Bull* 2:117–122. <https://doi.org/10.3969/j.issn.0441-3776.2005.02.011>

18. Wang Y (2008) Preparation and application of perovskite oxides. *Tianjin Chem Ind* 3:39–41. <https://doi.org/10.3969/j.issn.1008-1267.2008.03.014>
19. Ji T, Wang YK, Zhang HK, Li GH, Li ZF, Hao YY, Cui YX (2020) Application of hole transport materials to perovskite solar cells. *J Xi'an Jiaotong Univ* 10:63–76. <https://doi.org/10.7652/xjtxb202010008>
20. Sang LX, Li QW, Xu LX, Liu YM, Chong F (2008) Effect of doping  $\text{Cu}^{2+}$  on photocatalytic activity of perovskite oxides  $\text{LaFeO}_3$  for hydrogen evolution from water. *J Xi'an Jiaotong Univ* 5:626–629. <https://doi.org/10.3321/j.issn:0253-987X.2008.05.025>
21. Wang GY, Wang YJ, Liu QT (2007) Synthesis and photocatalytic activity of  $\text{NiO}/\text{Ba}_2\text{MgWO}_6$ . *J Xi'an Jiaotong Univ* 12:1499–1502. <https://doi.org/10.3321/j.issn:0253-987X.2007.12.026>
22. Nui XS, Cao ZM (2006) Progress in photocatalysis of perovskite oxides. *Chem Res Appl* 7:770–775. <https://doi.org/10.3969/j.issn.1004-1656.2006.07.004>
23. Bai XY, Ren YW, Yu Y, Zhang XK, Wang HL, Jiang WW, Wang N, Liu CQ, Liu SM, Ding WY (2021) Preparation, modification and application of  $\text{ABO}_3$  perovskite photocatalyst. *J Funct Mater Devices* 1:1–7
24. Fan WT, Tian J, Liu QJ (2009) Research progress in perovskite composite gas-sensitive materials. *Mater Rev* 14:358–361. <https://doi.org/10.3321/j.issn:1005-023X.2009.z2.106>
25. Shi C, Shao GJ, Hu J, Zhao BL, Lv YL (2008) Progress in nano-thin films of perovskite-type complex oxides. *Chin J Nonferrous Metals* 10:1893–1902. <https://doi.org/10.3321/j.issn:1004-0609.2008.10.023>
26. Albrecht KJ, Jackson GS, Braun RJ (2016) Thermodynamically consistent modeling of redox-stable perovskite oxides for thermochemical energy conversion and storage. *Appl Energy* 165:285–296. <https://doi.org/10.1016/j.apenergy.2015.11.098>
27. Imponenti L, Albrecht JK, Kharait R, Sanders MD, Jackson GS (2018) Redox cycles with doped calcium manganites for thermochemical energy storage to 1000 °C. *Appl Energy* 230:1–18. <https://doi.org/10.1016/j.apenergy.2018.08.044>
28. Bakken E, Norby T, Stølen S (2005) Nonstoichiometry and reductive decomposition of  $\text{CaMnO}_{3-\delta}$ . *Solid State Ionics* 1–2:217–223. <https://doi.org/10.1016/j.ssi.2004.07.001>
29. Bulfin B, Vieten J, Starr DE, Azarpira A, Zachäus C, Hävecker M, Skorupska K, Schmücker M, Roeba M, Sattler C (2017) Redox chemistry of  $\text{CaMnO}_{3-\delta}$  and  $\text{Ca}_{0.8}\text{Sr}_{0.2}\text{MnO}_{3-\delta}$  oxygen storage perovskites. *Mater Chem* 17:7912–7919. <https://doi.org/10.1039/C7TA00822H>
30. Gokon N, Yawata T, Bellan S, Kodama T, Cho H (2019) Thermochemical behavior of perovskite oxides based on  $\text{La}_x\text{Sr}_{1-x}(\text{Mn, Fe, Co})\text{O}_{3-\delta}$  and  $\text{Ba}_x\text{Sr}_{1-x}\text{CoO}_{3-\delta}$  redox system for thermochemical energy storage at high temperatures. *Energy* 171:971–980. <https://doi.org/10.1016/j.energy.2019.01.081>
31. Salles C, Steil M, Fouletier J, Duttine M, Wattiaux A, Marinha D (2019) Long-term stability of iron-doped calcium titanate  $\text{CaTi}_{0.9}\text{Fe}_{0.1}\text{O}_{3-\delta}$  oxygen transport membranes under non-reactive and reactive atmospheres. *J Membr Sci* 583:171–179. <https://doi.org/10.1016/j.memsci.2019.04.049>
32. Bak T, Nowotny J, Rekas M, Ringer S, Sorrell CC (2001) Defect chemistry and electrical properties of  $\text{La}_{1-x}\text{Sr}_x\text{CoO}_{3-\delta}$  III. Oxygen Nonstoichiometry. *Oxygen Nonstoichiometry* 7:380–387. <https://doi.org/10.1007/BF02373573>
33. Qiang JL, Wang DH, Hui SE (2022) Synthesis of  $\text{La}_{1-x}\text{Sr}_x\text{CoO}_{3-\delta}$  and its REDOX performance in air. *J Environ Chem Eng* 6:108794. <https://doi.org/10.1016/j.jece.2022.108794>
34. Qiang JL, Wang DH, Chu H, Hui SE (2023) experimental study on thermochemical energy storage of A-doped  $\text{LaCoO}_3$  perovskite oxides. *J Xi'an Jiaotong Univ* 3:1–13
35. Alhokbany N, Almotairi S, Ahmed J, Al-Saeedi SI, Ahamad T, Alshehri SM (2021) Investigation of structural and electrical properties of synthesized Sr-doped lanthanum cobaltite ( $\text{La}_{1-x}\text{Sr}_x\text{CoO}_3$ ) perovskite oxide. *J King Saud Univ-Sci* 4:101419
36. Gao DS, Fang ZG, Lu CH, Ni YR, Xu ZZ (2015) Synthesis and optical properties of perovskite-type oxide  $\text{Sm}_{0.5}\text{Sr}_{0.5}\text{CoO}_{3-\delta}$ . *Funct Mater* 5:05039–05042
37. Niu JR, Liu W, Dai HX, Zi XH, He H, Li PH (2006) Preparation and characterization of strontium doped Lanthanum cobaltite efficient nano catalyst with large specific surface area. *Sci Bull* 8:912–918. <https://doi.org/10.1360/CSB2006-51-8-912>
38. Liu XY, Zhang XJ, Yang SQ, Han J, Li YF, Zhang L, Gao ZX (2022) Study on wet oxidation of phenol catalyzed by  $\text{LaFeO}_3$  perovskite. *J Fuel Chem* 11:1491–1497. <https://doi.org/10.19906/j.cnki.JFCT.2022044>

39. Ishihara T, Fukui S, Nishiguchi H, Takita Y (2002) Mixed electronic-oxide ionic conductor of BaCoO<sub>3</sub> doped with La for cathode of intermediate temperature-operating solid oxide fuel cell. *Solid State Ionics* 152–153:609–613. [https://doi.org/10.1016/S0167-2738\(02\)00394-6](https://doi.org/10.1016/S0167-2738(02)00394-6)
40. Yang QH, Fu XX, Sang LX, Sun YH, Wang JZ (2003) Photocatalytic properties of perovskite-type LaFeO<sub>3</sub> and SrFeO<sub>3</sub>. *Silicate Bull* 3:15–18. <https://doi.org/10.3969/j.issn.1001-1625.2003.03.004>
41. Hari Prasad D, Park SY, Oh EO, Ji H, Kim HR, Yoon KJ, Son JW, Lee JH (2012) Synthesis of nanocrystalline La<sub>1-x</sub>Sr<sub>x</sub>CoO<sub>3-δ</sub> perovskite oxides by EDTA–citrate complexing process and its catalytic activity for soot oxidation. *Appl Catal A* 447–448:100–106. <https://doi.org/10.1016/j.apcata.2012.09.008>
42. Zhang J, Zhao HL, Cheng YF, Ding WZ (2009) Progress in A-site and B-site doped modified BaCoO<sub>3</sub> based oxygen permeable membrane materials. *Battery Bimonthly* 5:282–284

**Publisher's Note** Springer Nature remains neutral with regard to jurisdictional claims in published maps and institutional affiliations.

Springer Nature or its licensor (e.g. a society or other partner) holds exclusive rights to this article under a publishing agreement with the author(s) or other rightsholder(s); author self-archiving of the accepted manuscript version of this article is solely governed by the terms of such publishing agreement and applicable law.